IAES International Journal of Robotics and Automation (IJRA)
Vol. 15, No. 2, June 2026, pp. 397~414
ISSN: 2722-2586, DOI: 10.11591/ijra.v15i2.pp397-414

Robust and computationally efficient single-input fuzzy logic-enhanced nonlinear PID control for a pneumatic servo system

Khairun Najmi Kamaludin[1], Lokman Abdullah[1], Syed Najib Syed Salim[2], Zamberi Jamaludin[1], Mohd Nazmin Maslan[1], Mohd Shahrieel Mohd Aras[2], Mohd Fua'ad Rahmat[3], Arief Suardi Nur Chairat[4]
[1]Fakulti Teknologi dan Kejuruteraan Industri dan Pembuatan, Universiti Teknikal Malaysia Melaka, Durian Tunggal, Malaysia
[2]Fakulti Teknologi dan Kejuruteraan Elektrik, Universiti Teknikal Malaysia Melaka, Durian Tunggal, Malaysia
[3]Fakulti Kejuruteraan Elektrik, Universiti Teknologi Malaysia, Johor Bahru, Malaysia
[4]Department of Industrial Engineering, Institut Teknologi PLN, Jakarta, Indonesia

Article Info

Article history:

Received Dec 5, 2025
Revised Apr 9, 2026
Accepted Apr 16, 2026

Keywords:

Adaptive control
Friction compensation
Low-cost controller
Nonlinear PID
Robust control
Servo pneumatic
Single-input fuzzy logic

ABSTRACT

Precision and robustness are essential for any automation actuator. Due to the nonlinear characteristics of the pneumatic actuator, advanced nonlinear control algorithms provide exceptionally precise control but are sensitive to disturbances. Owing to this factor, an adaptive element is embedded into the control structure to obtain a robust strategy by integrating single input fuzzy logic (SIFL) with the nonlinear hyperbolic PID controller (T NPID). SIFL characterizes a variable rate in the function while reducing computational complexity against an equivalent classical fuzzy logic (FL) by up to 36.5%. The signed distance SIFL selection is also a novel structure that has never been applied in the pneumatics control field. The robustness of the controller is analysed via dynamic stiffness and validated by applying multiple load disturbances. The improvement gained for the T NPID+SIFL's transient rise time and multi-step IAE index under no load disturbance is 71.381% and 68.854%, respectively, compared with a classical sliding mode controller (SMC). Under a maximum 9 kg load disturbance (limited within the scope of this research), the T NPID+SIFL's IAE index performance obtained an improvement of 68.638%. When compared with a baseline nonlinear hyperbolic PID (NH PID) strategy under no load disturbance, the steady state error and overshoot also improved by 74.797% and 15.385%, respectively. The results show outstanding performance compared with a robust controller as well as a similar baseline nonlinear PID control. Asymptotic stability analysis, such as the asymptotic tracking region (ATR), will be able to consolidate the trajectory tracking performance together with the experimental validation of a smooth trajectory, simulating a real-time robotic actuator under movement control.

Corresponding Author:

Lokman Abdullah
Fakulti Teknologi dan Kejuruteraan Industri dan Pembuatan, Universiti Teknikal Malaysia Melaka
Melaka, Malaysia
Email: lokman@utem.edu.my

1. INTRODUCTION

Many industrial applications, such as those requiring manipulators, riveting machines, automobiles, pick-and-place devices, and others, extensively use pneumatic actuators. Pneumatic systems have a variety of benefits, including ease of maintenance, lower cost, and low heat generation under steady load [1]–[3]. Due

to these benefits, pneumatic actuators continue to attract significant research interest. However, achieving high precision and accuracy in performance presents several challenges. Nonlinear pneumatic actuators pose challenges to the control field with disturbances such as a wide dead zone, air compression nonlinearity, low damping, and frictional forces [4]. Internal friction force is widely agreed to be one of the critical disturbances in an actuator that affects the performance required to achieve precise positioning and trajectory tracking in a servo system [5], [6]. In a pneumatic actuator, friction occurs between the seal and the internal cylinder wall [6], [7]. According to a review by Saravanakumar *et al*. [8], friction force compensation has been predominantly addressed by researchers compared with other disturbances such as air pressure and dead zone effects, which indicates that it is a significant disturbance in this field.

Adaptive control strategies were adopted in pneumatic systems in the early 2000s [9]. Adaptive controllers are able to realise real-time online parameter estimation of linear and nonlinear time-varying systems to adapt to changes [10]. However, adaptive controllers are not widely explored in this field compared with PID-based and SMC-based strategies, as the formulation is relatively complex and the precision results are inferior. Adaptive controllers were designed using friction compensation methods by Gao and Feng [11], while the research by Farag and Azlan [12] did not focus on adaptivity in internal friction forces.

An extension of adaptive controllers is the adaptive robust controller (ARC). A comprehensive review of ARC is presented in [10], where the strategy is also proposed. Robustness criteria are added to the algorithm to ensure stability and improved precision. ARC was initially proposed as a general control concept [13], [14] and was later adapted to the pneumatic field [15], [16]. The strategy was further extended via the friction compensation method [17]. The sliding mode control (SMC) strategy has also been proven to be robust. Due to the formulation of SMC, the strategy is able to effectively compensate for friction because its core characteristic is that SMC neglects disturbances. However, this formulation requires precision during the modelling stage, as required by the strategy's equivalent control. SMC strategies in recent years were presented in several studies, such as [18], [19]. The only SMC strategies that have been found with friction compensation were reported by Soleymani *et al*. [7] and Hidalgo and Garcia [20]. While SMC offers both theoretical and experimental robustness, its reliance on precise modelling, tuning methods, and susceptibility to chattering limits its practical deployment in industry. In contrast, PID-based strategies—especially when enhanced with nonlinear or intelligent modules—offer a more adaptable and implementation-friendly solution, making them preferable for industrial control where simplicity, tuneability, and reliability are critical [21], [22]. Nonlinear PIDs include multi-rate nonlinear PID (MN-PID), self-regulating nonlinear PID (SN-PID), and the double nonlinear PI controller [23]. Studies integrating nonlinear PIDs with friction compensation modules were proposed in [24] and [25]. Previous research proposed an advanced nonlinear hyperbolic PID with friction compensation (T-NPID+F_{SS}) [26]. However, the strategy's robustness was not analysed or validated. For this reason, the contribution of this research extends the design and analysis of the T-NPID+F_{SS} by integrating an advanced, yet simplified and practical fuzzy logic design, namely single-input fuzzy logic (SIFL), to enhance the strategy's robustness.

A review of fuzzy logic in hydraulics and pneumatics control [27] highlights the increasing use of fuzzy structures. Prior studies employing the SIFL formulation proposed in [28] integrated it mainly into SMC's switching law, while other studies relied on classical two-input configurations that offer conventional performance. In contrast, this study adopts the more structured SIFL architecture introduced by Choi *et al*. [29], which incorporates a signed-distance parameter to generate a flexible control surface with lower computational complexity. This formulation has not yet been applied to precision servo pneumatic control. Therefore, integrating the signed-distance-based SIFL into a nonlinear PID framework addresses a clear research gap.

The rest of this paper is organised as follows. Section 2 explains the step-by-step procedure for analysing the prototype in detail, followed by the Results and Discussion in Section 3. Finally, Section 4 presents the conclusion and future recommendations.

2. METHOD

2.1. System setup and modelling

The servo pneumatic actuator system is modelled using the time-domain system identification method. Figure 1 and Table 1 show the experimental setup and the equipment used. The actuator system is communicated with the personal computer (PC) running MATLAB via a data acquisition (DAQ) box.

The process involves building mathematical models of dynamic systems from observed input-output data [30]. Figure 2 shows the modelling process of the plant. As this research applies the friction compensation method, the flowchart also presents the strategy for modelling the plant with friction, which was previously explained by Kamaludin *et al*. [26]. The experimental plant requires the signal to be sent continuously; therefore, a continuous transfer function is presented for modelling, as shown in equation (1),

and is used during the design and simulation stages. The transfer function form also simplifies the stability analysis using the Popov theorem [31]. Once system identification is completed, identification and modelling of the static and dynamic friction are performed and integrated into the plant model. The validation of the model with friction achieves a best fit to the experimental data of at least 90%.

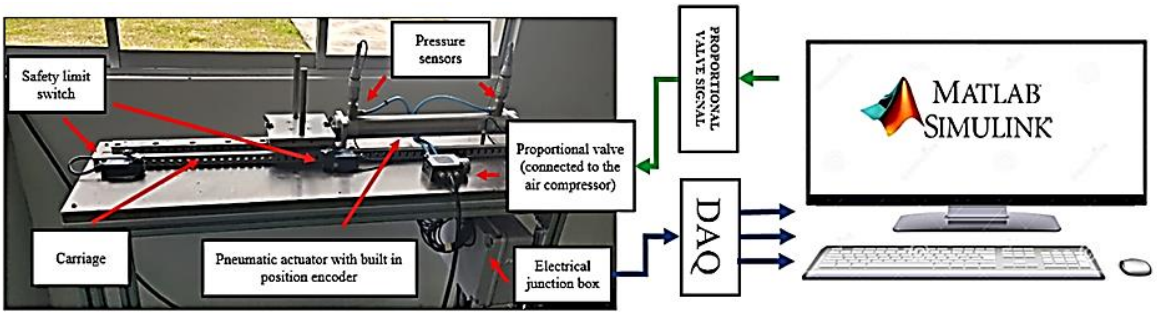

Figure 1. Servo pneumatic system experimental setup

Table 1. Equipment for the system

Equipment	Model Number	Specification
Proportional valve	Enfield LS-V15s	5/3 port, 0-10 Volts
Pneumatic actuator with integrated position encoder	Enfield ACTB-200-S10200	304.80 mm stroke length, 0-10 Volts
Pressure sensor	Gems Sensor 1200SGG	0 to 10 volts, 0-150 PSI
Safety limit switch	Tezuo AZ8104	Contact on (0/1 digital signal)
DAQ Box	National Instrument PCI-6221	37 Pin PCI interfacing
MATLAB/Simulink	Version 2016b	64 bits

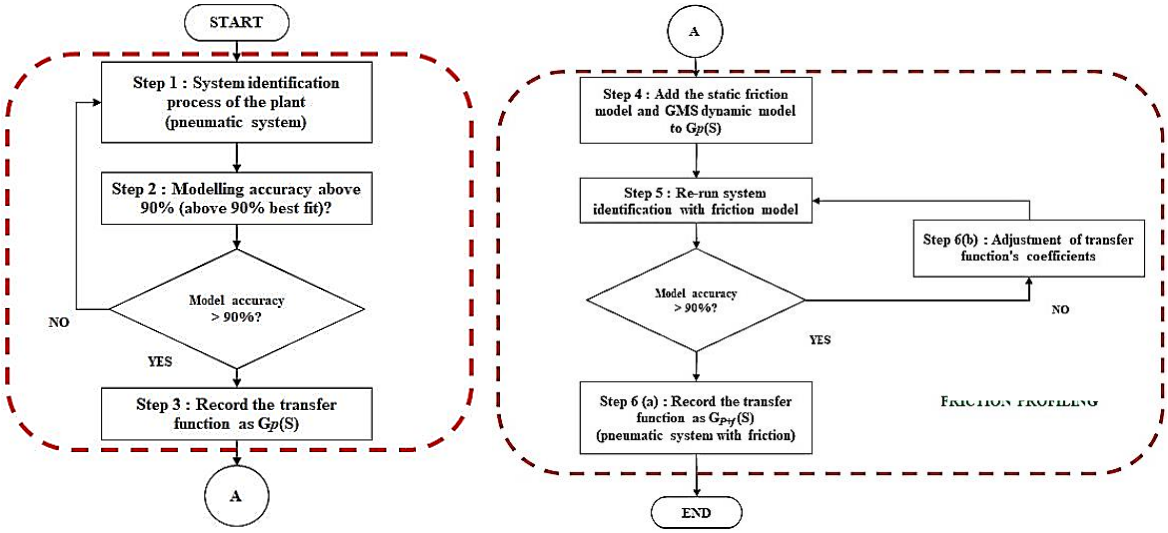

Figure 2. System modelling with friction flowchart

$$G(s) = \frac{0.03468s^2+0.1468s-0.002041}{s^3+0.2921s^2+0.02056s+0.000085} \quad (1)$$

The static friction parameters are tabulated in Table 2. Adjustment of the parameters is based on the model's best fit to the data. The parameters were adjusted from the previously reported values [26], as the research achieved a correlation best fit of 57.45%, while the latest parameters (as shown in Table 2) achieved a best fit of 64.89%. This represents the highest best-fit value able to be achieved from the current experimental internal friction force readings. To further increase the best fit of the current static friction model, the implementation of an advanced noise filter or replacement of the pressure and displacement sensors with lower-noise alternatives to obtain less distorted experimental data is proposed as a future scope of this research, as suggested by Qian *et al*. [10]. Higher accuracy of the friction model, or improved friction

modelling such as dynamic friction model compensation (especially at lower velocity analysis), is able to result in better precision control [7].

Table 2. Static friction parameter value

Static Friction Parameter	Parameter value
Coulomb friction, F_c (Newton)	18.50
Stribeck friction, F_s (Newton)	27.90
Stribeck velocity, V_s (mm/s)	1.65
Viscous friction, F_v (Newton·second/mm)	0.60

The dynamic friction modelling adapts the generalised Maxwell Slip (GMS) friction model, which requires extraction of the virgin curve from the plotted hysteresis of the friction force versus displacement graph. The GMS method was previously applied to other actuator systems [32] and was subsequently carried over to pneumatic actuators [33]. The transfer function's best fit obtained before the inclusion of the friction models is 94.27%. Including both the static and dynamic friction models yields a best fit of 92.96%. The drop in best fit is anticipated due to the inclusion of internal friction force models. Following the flowchart, the latter model does not drop below 90% of the measured data; therefore, the transfer function does not require coefficient adjustment. The transfer function with the friction models is applied in the methodology [34]. The low effect of the friction model on the overall system is due to the conversion of the friction force to voltage in the modelling structure, where the friction force is multiplied by the k_f. k_f constant, valued at −1/2020 [26], resulting in small voltage values in simulation. Although the friction force is relatively low compared with other mechanical actuators, the effect of the disturbance is highly significant in precision control [35].

2.2. Design of triple nonlinear-hyperbolic PID controller with SIFL (T-NPID+SIFL)

The T-NPID+SIFL is based on the T-NPID controller. The design of the T-NPID follows the structure presented in [26], which is developed based on the Popov stability region. A nonlinear hyperbolic algorithm is adapted for each PID gain, K_P, K_I, and K_D. The nonlinear gains are presented in (2) to (4), where the multiplied error follows the condition defined in (5). An asymptotic tracking behaviour analysis using Lyapunov's indirect method was also presented in [36], consolidating the stability of the controller. The parameters of the T-NPID were optimised using particle swarm optimisation (PSO), as similarly presented in [37], and the resulting parameters are tabulated in Table 3.

$$K_p(e) = 1 + f \times [1 - \text{sech}(g \times e_p)] \tag{2}$$

$$K_I(e) = 1 \div [p + q \times (1 - \text{sech}(r \times e_I))] \tag{3}$$

$$K_D(e) = 1 \div [a + b \times (1 - \text{sech}(c \times e_D))] \tag{4}$$

$$error, e_{P,I,D} = \begin{cases} e & |e| \le e_{max} \\ e_{max} \cdot sign(e) & |e| > e_{max} \end{cases} \tag{5}$$

Table 3. PSO optimized T-NPID parameter

Parameter		Value
Nonlinear Hyperbolic Function at Proportional Gain, P	f	3.042
	g	9.045
	e_P	0.5
Nonlinear Hyperbolic Function at Integral Gain, I	p	1
	q	33.200
	r	34.000
	e_I	0.5
Nonlinear Hyperbolic Function at Derivative Gain, D	a	1
	b	9.867
	c	6.333
	e_D	0.5

The design of the T-NPID+SIFL integrates SIFL as a control mechanism to vary one of the parameters in the nonlinear function. This integration improves the controller's flexibility and enables multiple gain variations. This concept has been proven by Salim [4]. For the $K_P(e)$ two parameters are

available for rate variation, namely f and g. The effects of varying either parameter *f* or *g* in the formulation are visualised in Figure 3. Figure 3(a) shows the variable *g*, and Figure 3(b) shows the variable f. From visual observation, the variable *f* produces a more aggressive response as the increase in nonlinear gain is narrower from the system's zero error *e*, as denoted in Figure 3(b). With reference to the research by Salim [4], parameter multiplication of the error is used for rate variation. Therefore, this research applies the rate variation using SIFL to the parameter *g* from (2). Figure 4 shows the schematic diagram of the control strategy. Since this research applies the friction compensation method, a static friction compensation feedback module (F_{SS}) is adapted to all included control strategies. The significance of the module is well explained in [26].

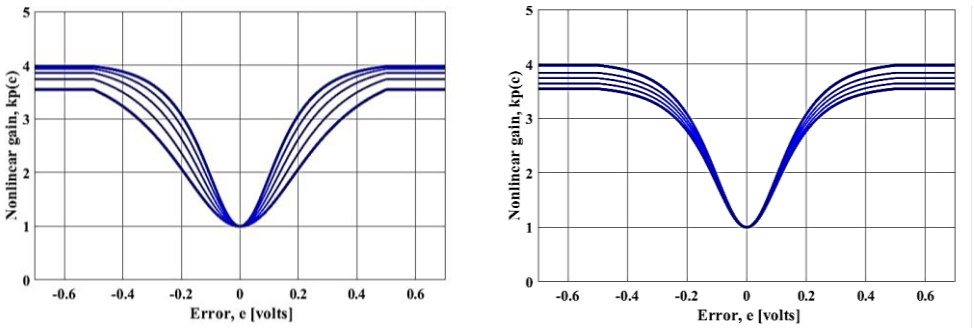

(a) (b)

Figure 3. Nonlinear hyperbolic gain with variable parameter (a) *g* and (b) *f*

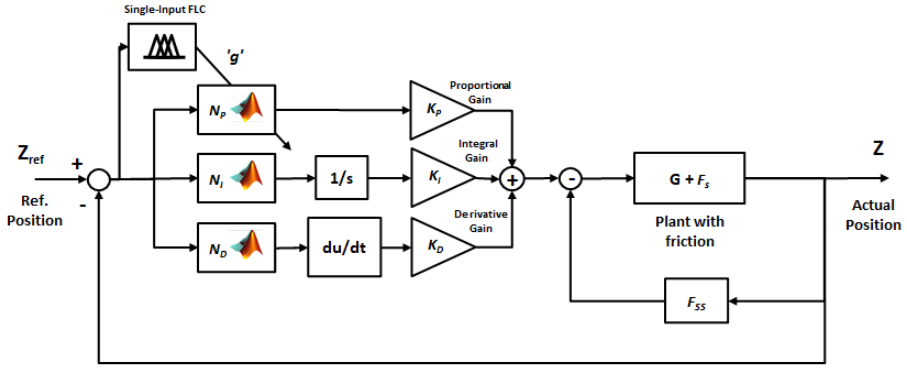

Figure 4. T-NPID+SIFL control strategy schematic diagram, with F_{SS} friction compensation module

Fuzzy logic is able to be initially designed linguistically. The linguistic expression of the system's error range is defined in equations (6) and (8), while the membership functions, α are defined in (7) and (9). The error range is set from zero (0) to one (1), whereas the output of the fuzzy logic system is set from zero (0) to negative one (-1).

$$|e_x| \in \{|e_1|, |e_2|, |e_3|, \dots\dots\dots\dots\dots\dots, |e_n|\} \quad (6)$$

$$\alpha_x \in \{\alpha_1, \alpha_2, \alpha_3, \dots\dots\dots\dots\dots\dots, \Delta|\alpha_n|\} \quad (7)$$

$$e = \{e_x|e_x \to [0,1] \quad \forall_x = 0, \dots\dots\dots, 1\} \quad (8)$$

$$\alpha = \{\alpha_x|\alpha_x \to [0,-1] \quad \forall_x = 0, \dots\dots\dots\dots, -1\} \quad (9)$$

The conversion of fuzzy logic to single-input fuzzy logic is based on the approach presented in [29]. In conventional dual-input fuzzy logic, the inputs consist of the tracking error, *e*, and the error rate, Δe. The main advantage of the single-input fuzzy logic (SIFL) scheme compared to the standard fuzzy logic

controller is the elimination of the membership function associated with Δe. The error rate, Δe, is transformed into the switching function s_1, as shown in equation (10) and (11). The input formulation described in [29] is given in (12), where d_1 represents the single input. The relationship aggressiveness between e and Δe is tuned by the signed-distance parameter, λ. Consequently, the number of membership functions (MFs) is able to be reduced from 49 sets (α^2) to only 7 sets. The SIFL membership functions are tabulated in Table 4.

$$s_1 : \Delta e_n + \lambda e_n \tag{10}$$

$$d_1 = [(e_n - e_{n+1})^2 + (\Delta e_n - \Delta e_{n+1})^2]^{\frac{1}{2}} \tag{11}$$

$$\therefore\ d_1 = \frac{|\dot{e}_1 + \lambda e_1|}{\sqrt{1+\lambda^2}} \tag{12}$$

The design of the asymmetrical SIFL follows the approach by Taeed *et al*. [38]. The symmetrical and asymmetrical designs are able to be performed via the SIFL method. A rule table based on the input (error) of the system is created, as tabulated in Table 4. For a symmetrical SIFL, the rule table is the same. The difference is the MF values that are able to be changed in MATLAB's Fuzzy Logic Controller application. Figure 5 shows the triangular membership function skewed towards a more significant error input, which means the SIFL will respond more when the system error is more significant. The output membership function is a Sugeno type and is skewed towards a more significant negative output, denoting the same condition (also shown in Figure 5). The linguistic expression from (6) to (9) and the condition stated in the last two statements yield the rule table with the membership values in Table 4 [39].

Table 4. Rule table for SIFL

Input, e	LNB	LS1	LS2	LM	LB1	LB2	LB3
MF value	1, 0.1	0, 0.5, 0.6	0.1, 0.7, 0.85	0.6, 0.85, 0.9	0.85, 0.9, 0.95	0.9, 0.95, 1	0.95, 1
Output, α	Z	S1	S2	M	B1	B2	B3
MF value	0	-0.35	-0.70	-0.85	-0.90	-0.95	-1

The control surface in Figure 5 shows the SIFL relation between the input and output, and the whole figure is known as the piecewise linear function (PWL). For a dual input fuzzy logic, a three-dimensional control surface is usually presented, but due to the simplicity of the SIFL, a two-dimensional control surface is generated. The design of the SIFL also reduces calculation complexity and time. A simple simulation comparing FL and SIFL in 10 seconds produced the calculation time shown in Figure 6. FL managed to compute the output with an average of 3.259 seconds, while the SIFL performed with an average of 2.068 seconds, a reduction of 36.5%. The simulation agrees with the study by Salam *et al*. [40]. Consolidating the claim of computational savings, the C code (.c) generated via Simulink Coder yielded a 34.38% reduction in logic lines for the SIFL controller compared to classical fuzzy logic (273 versus 416 lines). The corresponding header files (.h) also saw a 7.04% reduction. The reduction in both programming logic lines aligns with the reduction of fuzzy rules from forty-nine to seven and confirms the structural simplicity of the single-input fuzzy logic design. A few samples of an asymmetric SIFL MATLAB file are available at GitHub (https://github.com/nzkhaish-lab/SIFLC_forPUBLIC) or fuzzy logic designers to further explore.

To adapt the *'g'* parameter in the nonlinear K_P function according to the SIFL output and simplify the tuning method, a simple mathematical conversion is performed before and after the SIFL module. For the SIFL input, if the error is lower than e_{max}, the error from the system is ratioed to the e_{max} value (from the nonlinear hyperbolic function, 0.5) and multiplied with the maximum of the SIFL input, e_x, as shown in (6). The value g is extracted from Table 3, while g_{min} is tuned by reducing the g and observing the steady-state error performance. When the error changes, the value reduction halts and is recorded as g_{min}. In this case, g_{min} is 4.5. Using (13) and (14) adaptation, the MF function of the SIFL does not require to be constantly changed during tuning, where only g_{min} is sufficient to be adjusted.

$$e_n = e_{input} = \begin{cases} \frac{e_{volts}}{e_{max}} \times (Max\ e_x) & e \le e_{max} \\ e_{max} \times Max\ e_x & e > e_{max} \end{cases} \tag{13}$$

$$variale\ `g' = g_{SIFL} = g_{min} + [(g - g_{min}) \times \alpha] \tag{14}$$

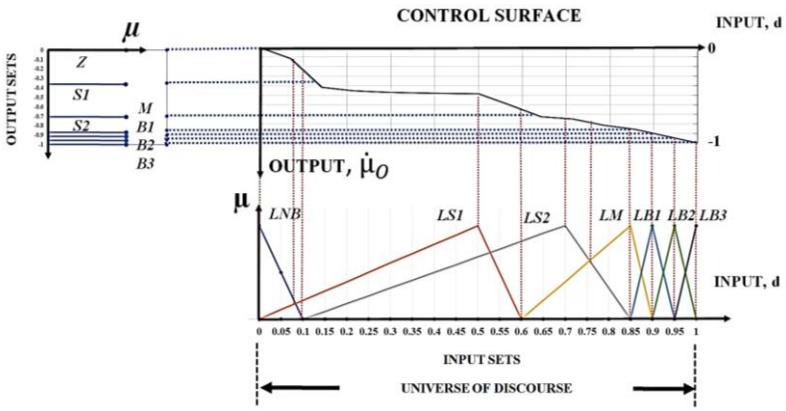

Figure 5. SIFL input-output and the control surface

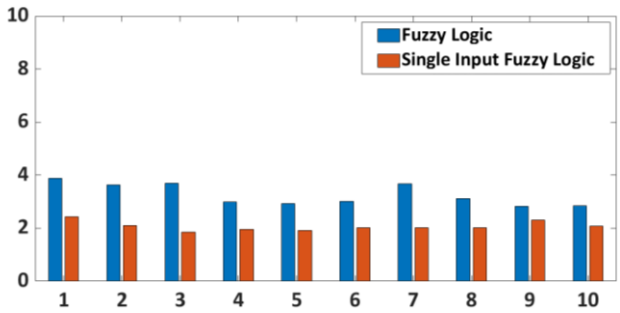

Figure 6. Simulation time comparison between FL and SIFL

Figure 7 shows the nonlinear functions for T-NPID+SIFL. The SIFL, based on its design, affects the K_P nonlinear function. The nonlinear gains for K_P range from the minimum to the maximum of the variable g value, controlled by the SIFL module; therefore, the visual of the K_P function is shown in the figure. g_{min} is the lowest blue line, while g (the maximum value) is the highest blue line, as denoted in Figure 7. A T-NPID without the SIFL will only have the g line. Since $K(e_{max})$ is not bounded by any value, and the g value only decreases from the initial value, T-NPID+SIFL is stable according to the Popov stability theorem.

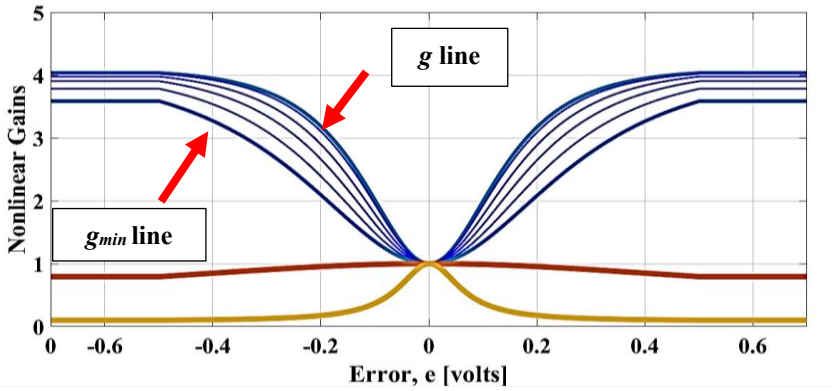

Figure 7. T-NPID+SIFL nonlinear functions

2.3. Dynamic stiffness of NH-PID, T-NPID, and T-NPID+SIFL

Dynamic stiffness is an essential measure of system performance in rejecting disturbances across different frequencies [42]. The dynamic stiffness of a nonlinear PID controller is the inverse of the compliance function, as shown in (15).

$$Dynamic\ stiffness, \frac{D(s)}{Z(s)} = \frac{1+N-PID\cdot\hat{G}}{\hat{G}/k_f} \quad (15)$$

$$Force\ to\ voltage\ constant,\ k_f = \frac{V}{f} \quad (16)$$

The pneumatic system is given a band-limited white noise signal as a disturbance input and measured for the output position. The dynamic stiffness is able to be approximated using the H_1 or H_2 estimator. Given that white noise exists at the system output (position encoder) and the input signal is clean except for MATLAB-generated excitation, the H_1 estimator is most appropriate for estimating the dynamic stiffness of this system. The H_2 estimator, in contrast, is best when additional noise is primarily at the input [28]. Figure 8 shows the frequency response function of the dynamic stiffness analysis for the three controllers.

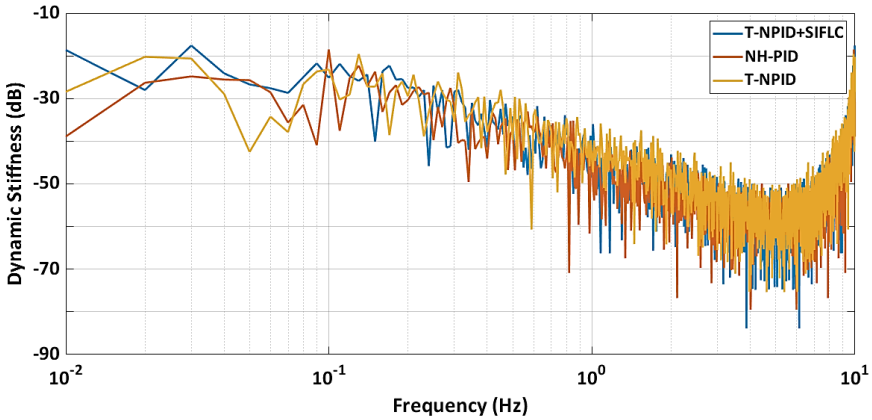

Figure 8. Comparison of the control strategies dynamic stiffness

The stiffness obtained in decibels (dB) is converted to forces in Newton. The novel controller demonstrated a slight improvement in dynamic stiffness in comparison to other controllers, where the T-NPID+SIFL has the lowest stiffness at higher frequencies and the highest stiffness at lower frequencies, as tabulated in Table 5. The results show that T-NPID+SIFL has the highest stiffness at low frequencies, which implies improved disturbance rejection capacity to position deviations under slow dynamic changes. This enhanced low-speed rigidity directly contributes to better trajectory tracking accuracy in precision applications, particularly where slow actuation is required.

Table 5. The dynamic stiffness results for each control strategy

Control strategy	Lower frequency dynamic stiffness		Higher frequency dynamic stiffness	
	Stiffness value ($\times10^{-5}$ Nm)	Frequency (Hz)	Stiffness value ($\times10^{-5}$ Nm)	Frequency (Hz)
NH-PID+F_{SS}	11,882.285	0.010	10.594	3.866
T-NPID+F_{SS}	10,501.105	0.130	17.065	5.354
T-NPID+SIFL+F_{SS}	13,219.347	0.030	6.396	3.866

3. RESULTS AND DISCUSSION

3.1. Simulation results

For any precise positioning actuator, either step positioning or trajectory tracking analysis (or both) must be performed as the numerical analysis procedure [41], [42]. For this research, two types of desired output were given to the control strategy to analyse each control strategy's precise positioning performance: a 100 mm step input and a multiple-steps (multi-step) positioning. The transient response and the steady-state error are able to be obtained from the step input, and the multi-step input will extend the result from the single-step performance. Table 6 presents the steady-state performance, and Table 7 tabulates the transient responses of each control strategy.

T-NPID and T-NPID+SIFL are not expected to outperform NH-PID drastically due to the nonlinearity of all the strategies. The nonlinearity of the controllers, even the base NH-PID, is able to deal

with the system's nonlinearity. Figure 9 shows the SIFL in action, where the error, *e* is extracted from the step positioning, and reference to the error, static *g* (from the T-NPID algorithm), and variable, *g* is presented. The SIFL module adjusts '*g' b*ased on the error and the SIFL module processing. The figure shows that *g* for the normal T-NPID is a straight line (dotted blue line) as opposed to the variable line (brown line) of the variable *g*. It is observed in the experimental results that when *g* is incorrect, the steady state error increases. It means that the desired position is not achieved.

Table 6. Steady-state simulation results for each control strategy

Steady-state parameter	NH-PID+F_{SS}	T-NPID+F_{SS}	T-NPID +SIFL+F_{SS}
Desired output, DO (mm)	100	100	100
Actual output, AO (mm)	99.593	99.999	99.998
Steady-state error, SSE (mm)	0.407	0.001	0.002
% Steady-state error, %SSE (%)	0.407	0.001	0.002

Table 7. Transient response simulation results for each control strategy

Transient response parameter	NH-PID+F_{SS}	T-NPID+F_{SS}	T-NPID+SIFL+F_{SS}
Rise time, T_R (seconds)	0.929	0.921	0.937
Percent overshoot, %OS (%)	2.60	2.10	2.20
Maximum overshoot, C_{MAX} (mm)	102.60	102.10	102.20
Peak time, T_P (seconds)	1.645	1.596	1.599
Settling time, T_S (seconds)	1.225	1.229	1.234
Dead time, T_D (seconds)	0.020	0.020	0.020

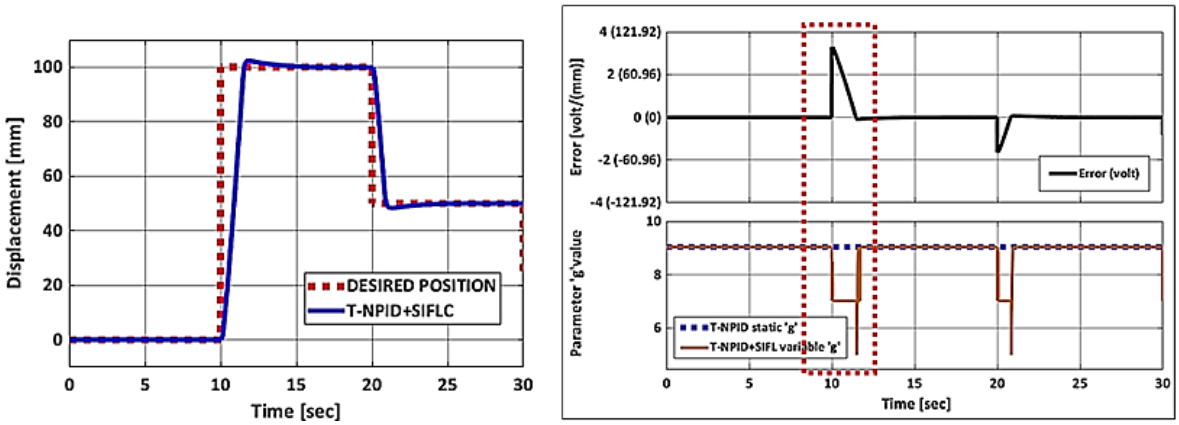

Figure 9. Adaptive and variable '*g*' value from the nonlinear K_P function

3.2. Experimental results and robustness test results

The actuator fixture is loaded with external load disturbance for the robustness test, as Figure 10 shows. The maximum available load for the system is 9 kilograms (kg), incremented by 1 kg load. To test the robustness, each control strategy is loaded incrementally with 1 kg, 5 kg, and 9 kg.

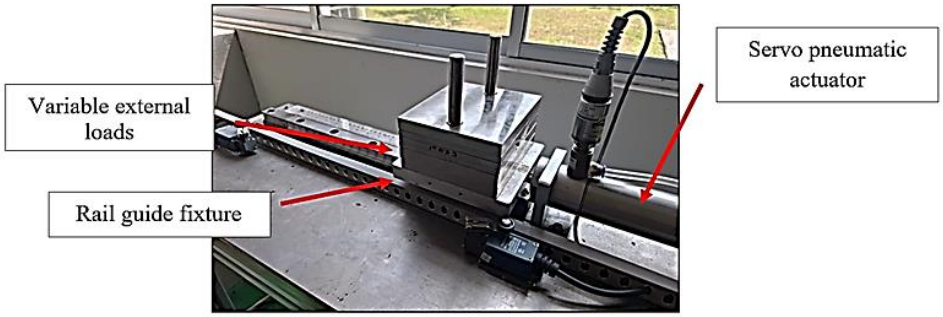

Figure 10. Pneumatic actuator fixture with external loading

A classical robust controller, sliding mode control (SMC), is added for performance benchmarking in the experimental and robustness tests. Figures 11(a) and 11(b) show robustness to the external load disturbances for SMC and NH-PID, respectively. Figures 12(a) and 12(b) shows the T-NPID controller and T-NPID+SIFL, respectively. Figures 11(b) and 12(a) shows that the controllers are unstable at 5 kg and 9 kg with oscillations, while Figures 11(a) and 12(b), SMC and T-NPID+SIFL respectively, shows no significant oscillations and are stable. Tables 8 and 9 tabulate the steady-state and transient responses, respectively. For NH-PID and T-NPID, the controllers are able to withstand only up to 1 kg. The loading of 5 kg and 9 kg will cause the controller to oscillate vigorously when trying to maintain at the desired position. T-NPID+SIFL is able to be robust until 9 kg, just as the benchmark SMC controller performs. SMC's transient response is very slow compared to T-NPID+SIFL, and this is where the latter strategy excels. Robustness is achieved by T-NPID+SIFL, while maintaining the transient response performance.

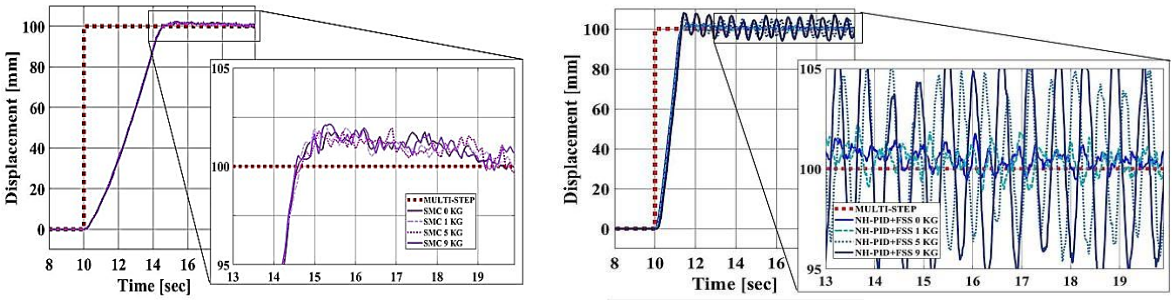

(a) (b)

Figure 11. Robust test of control strategies (a) SMC, and (b) NH-PID+F_{SS}

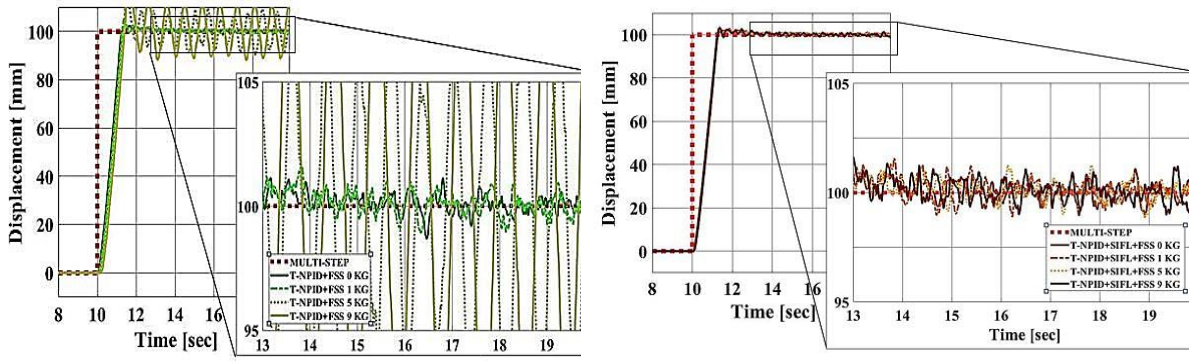

(a) (b)

Figure 12. Robust test of control strategies (a) T-NPID+F_{SS}, and (b) T-NPID+SIFL+F_{SS}

Table 8. Steady-state experimental results for each control strategy with external load disturbance

Additional external load disturbance	SMC		NH-PID +F_{SS}		T-NPID +F_{SS}		T-NPID +SIFL +F_{SS}	
0 kg (No load disturbance)	DO (mm)	100	DO (mm)	100	DO (mm)	100	DO (mm)	100
	AO (mm)	100.85	AO (mm)	100.82	AO (mm)	99.67	AO (mm)	99.66
	SSE (mm)	0.85	SSE (mm)	0.82	SSE (mm)	0.33	SSE (mm)	0.34
	%SSE (%)	0.85	%SSE (%)	0.82	%SSE (%)	0.33	%SSE (%)	0.34
1 kg	DO (mm)	100	DO (mm)	100	DO (mm)	100	DO (mm)	100
	AO (mm)	100.78	AO (mm)	101.23	AO (mm)	99.56	AO (mm)	99.69
	SSE (mm)	0.78	SSE (mm)	1.23	SSE (mm)	0.46	SSE (mm)	0.31
	%SSE (%)	0.78	%SSE (%)	1.23	%SSE (%)	0.46	%SSE (%)	0.31
5 kg	DO (mm)	100	**Unstable**		**Unstable**		DO (mm)	100
	AO (mm)	101.03	**(Oscillates)**		**(Oscillates)**		AO (mm)	100.31
	SSE (mm)	1.03					SSE (mm)	0.31
	%SSE (%)	1.03					%SSE (%)	0.31
9 kg	DO (mm)	100	**Unstable**		**Unstable**		DO (mm)	100
	AO (mm)	100.94	**(Oscillates)**		**(Oscillates)**		AO (mm)	100.92
	SSE (mm)	0.94					SSE (mm)	0.92
	%SSE (%)	0.94					%SSE (%)	0.92

Table 9. Transient response experimental results for each control strategy with external load disturbance

Additional weight	SMC		NH-PID $+F_{SS}$		T-NPID $+F_{SS}$		T-NPID+SIFL $+F_{SS}$	
0 kg (No external load)	T_R (s)	3.274	T_R (s)	0.929	T_R (s)	0.921	T_R (s)	0.937
	%OS (%)	1.89	%OS (%)	2.60	%OS (%)	2.10	%OS (%)	2.20
	C_{MAX} (mm)	101.89	C_{MAX} (mm)	102.60	C_{MAX} (mm)	102.10	C_{MAX} (mm)	102.20
	T_p (s)	16.202	T_p (s)	1.645	T_p (s)	1.596	T_p (s)	1.599
	T_S (s)	4.251	T_S (s)	1.225	T_S (s)	1.229	T_S (s)	1.234
	T_D (s)	0.053	T_D (s)	0.059	T_D (s)	0.044	T_D (s)	0.045
1 kg	T_R (s)	3.211	T_R (s)	0.941	T_R (s)	0.933	T_R (s)	0.941
	%OS (%)	1.93	%OS (%)	2.73	%OS (%)	3.01	%OS (%)	1.90
	C_{MAX} (mm)	101.93	C_{MAX} (mm)	102.73	C_{MAX} (mm)	103.01	C_{MAX} (mm)	101.90
	T_p (s)	17.413	T_p (s)	1.638	T_P (s)	1.601	T_P (s)	1.610
	T_S (s)	4.177	T_S (s)	1.420	T_S (s)	1.388	T_S (s)	1.255
	T_D (s)	0.059	T_D (s)	0.068	T_D (s)	0.031	T_D (s)	0.032
5 kg	T_R (s)	3.286	**Unstable**		**Unstable**		T_R (s)	0.950
	%OS (%)	1.75	**(Oscillates)**		**(Oscillates)**		%OS (%)	2.60
	C_{MAX} (mm)	101.75					C_{MAX} (mm)	102.6
	T_p (s)	16.022					T_P (s)	1.575
	T_S (s)	4.222					T_S (s)	1.243
	T_D (s)	0.055					T_D (s)	0.029
9 kg	T_R (s)	3.301	**Unstable**		**Unstable**		T_R (s)	0.939
	%OS (%)	1.67	**(Oscillates)**		**(Oscillates)**		%OS (%)	2.30
	C_{MAX} (mm)	101.67					C_{MAX} (mm)	102.30
	T_p (s)	15.991					T_P (s)	0.961
	T_S (s)	4.333					T_S (s)	1.310
	T_D (s)	0.061					T_D (s)	0.038

Figure 13 shows the experimental multi-step performances of all the control strategies. The multi-step consists of short, medium, and long strokes, both positive and negative displacements to evaluate precise positioning. Although each step is able to extract the transient response and steady-state error analysis, the accumulated errors are able to conclude the performance. Integral absolute error (IAE) and integral square error (ISE) are performance metrics used in control systems to evaluate the total accumulated error over time, as presented by (17) and (18), ensuring precise regulation [4]. IAE offers a more balanced view of persistent deviations, whereas *ISE* disproportionately penalizes large transient errors. This research focuses on achieving steady-state precision; therefore, *IAE* is applied rather than ISE. The final T-NPID+SIFL is the only controller (on top of the benchmarked SMC) expected to withstand up to the maximum disturbance load. Table 10 tabulates the *IAE* results for each strategy with the load disturbances. NH-PID and T-NPID are unstable at 5 kg and 9 kg. SMC and T-NPID+SIFL maintained the performance until the end.

$$IAE = \int_0^\infty |r(t) - y(t)|dt \tag{17}$$

$$ISE = \int_0^\infty |r(t) - y(t)|^2 dt \tag{18}$$

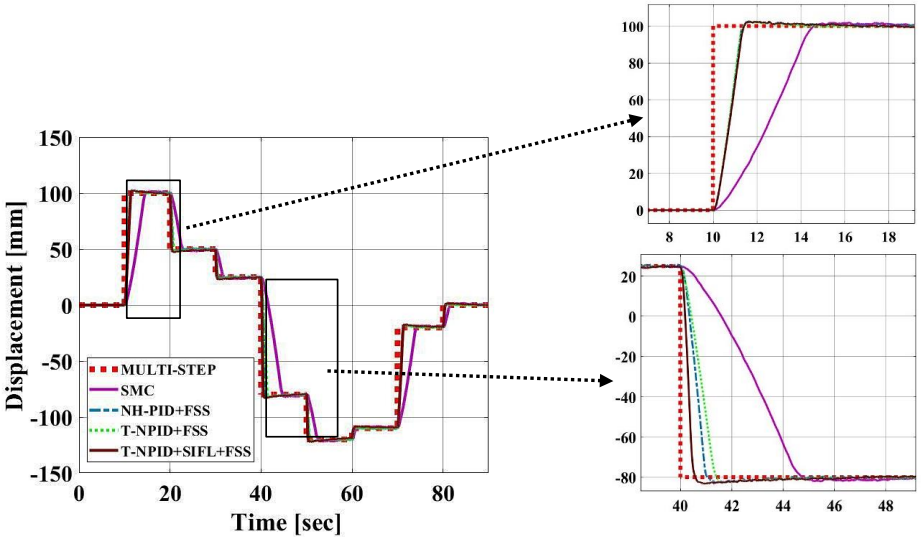

Figure 13. Experimental multi-step performance of NH-PID, T-NPID, T-NPID+SIFL and SMC

Table 10. IAE results for multi-step robustness

Additional external load disturbance	SMC	NH-PID $+F_{SS}$	T-NPID $+F_{SS}$	T-NPID+SIFL $+F_{SS}$
0 kg	870.462	282.742	269.982	271.113
1 kg	866.520	288.331	289.462	273.264
5 kg	867.273	**Unstable (Oscillates)**	**Unstable (Oscillates)**	273.339
9 kg	868.795	**Unstable (Oscillates)**	**Unstable (Oscillates)**	272.475

Table 11 tabulates the improvement gains of each control strategy at no loading disturbance, with SMC as the reference benchmark controller. The improvement gains are calculated using the percent improvement value reduction shown in equation (19). A few minus gains were seen (non-improvement), in the overshoot (OS). SMC usually does not overshoot due to the formulation and slow response time. And therefore, the nonlinear PIDs are not better in OS. However, the other measured parameters show huge improvement. The performance of T-NPID+SIFL continues until 9 kg load disturbance, as tabulated in Table 12. Overshoot increases slightly for the final strategy. NH-PID and T-NPID are unable to gain any improvement as instability.

$$\text{Percent improved value } \textit{reduction}\,(\%) = \left[\frac{Benchmark\ value - Improved\ value}{|Benchmark\ value|}\right] \times 100\% \quad (19)$$

Table 11. Error reduction improvement for 0 kg (SMC as reference)

Parameter	Control strategy				Error reduction (%)			
	SMC	NH-PID +Fss	T-NPID +Fss	T-NPID+SIFL +Fss	SMC	NH-PID +Fss	T-NPID +Fss	T-NPID+SIFL +Fss
SSE	0.85	0.82	0.33	0.34	**-Ref-**	3.529	61.176	60.000
T_R	3.274	0.929	0.921	0.937	**-Ref-**	71.625	71.869	71.381
% OS	1.89	2.60	2.10	2.20	**-Ref-**	-37.566	-11.111	-16.402
T_S	4.251	1.225	1.229	1.234	**-Ref-**	71.183	71.089	70.972
IAE	870.462	282.742	269.982	271.113	**-Ref-**	67.518	68.984	68.854

Table 12. Error reduction improvement for 9 kg (SMC as reference)

Parameter	Control strategy				Error Reduction (%)			
	SMC	NH-PID +Fss	T-NPID +Fss	T-NPID+SIFL +Fss	SMC	NH-PID +Fss	T-NPID +Fss	T-NPID+SIFL +Fss
SSE	0.94	**-NA-**	**-NA-**	0.92	**-Ref-**	**-NA-**	**-NA-**	2.128
T_R	3.301	**-NA-**	**-NA-**	0.939	**-Ref-**	**-NA-**	**-NA-**	71.554
% OS	1.67	**-NA-**	**-NA-**	2.30	**-Ref-**	**-NA-**	**-NA-**	-37.725
T_S	4.333	**-NA-**	**-NA-**	1.310	**-Ref-**	**-NA-**	**-NA-**	69.767
IAE	868.795	**-NA-**	**-NA-**	272.475	**-Ref-**	**-NA-**	**-NA-**	68.638

Table 13 tabulates the performance improvement when NH-PID is the reference, removing SMC. The steady-state errors are improved significantly, which shows that the triple nonlinear hyperbolic works to reduce the error. A few non-improvements are observed, such as the T-NPID+SIFL rise time TR, and both of the T-NPIDs settling time TS. However, the values are below 1 percent which suggest that it is only distortion of data during capturing due to noise and is not significant. For 9 kg loading, the improvement table is not presentable as the base NH-PID is unstable.

Table 13. Error reduction improvement for 0 kg (NH-PID as reference)

Parameter	Control strategy			Error Reduction (%)		
	NH-PID +Fss	T-NPID +Fss	T-NPID+SIFL+Fss	NH-PID +Fss	T-NPID +Fss	T-NPID+SIFL +Fss
SSE	1.230	0.460	0.310	**-Ref-**	62.602	74.797
T_R	0.929	0.921	0.931	**-Ref-**	0.861	-0.215
% OS	2.600	2.100	2.200	**-Ref-**	19.231	15.385
T_S	1.225	1.229	1.234	**-Ref-**	-0.327	-0.735
IAE	282.742	269.982	271.113	**-Ref-**	4.512	4.113

3.3. Discussions

The performances are on par with the precise positioning performance of every presented nonlinear hyperbolic controller. Even the base NH-PID performs adequately. The steady-state error does show a slight

improvement for the T-NPID over the NH-PID. Over a more extensive multi-step performance analysis, the total error is lesser, which is shown to be better for the T-NPIDs. The final novel controller shows superiority when the maximum load disturbance is applied to the actuator. T-NPID+SIFL is able to hold the transient responses and the steady-state results and perform precise multi-step positioning better than the two controllers. The variable rate of a new function has also been shown previously by Salim [4], using the classical FL as shown in Figure 14. However, no adaptation formulation prior to the FL module invites complexity to tune the module. The proposed T-NPID+SIFL overcomes the disadvantage by formulating a simple adaptation module as in (14), simplifying the requirement to adjust only parameters g and g_{min}. Furthermore, the streamlined structure of the SIFL significantly reduces computational burden and tuning effort, offering a more efficient and adaptable alternative to classical FLs—particularly in real-time applications.

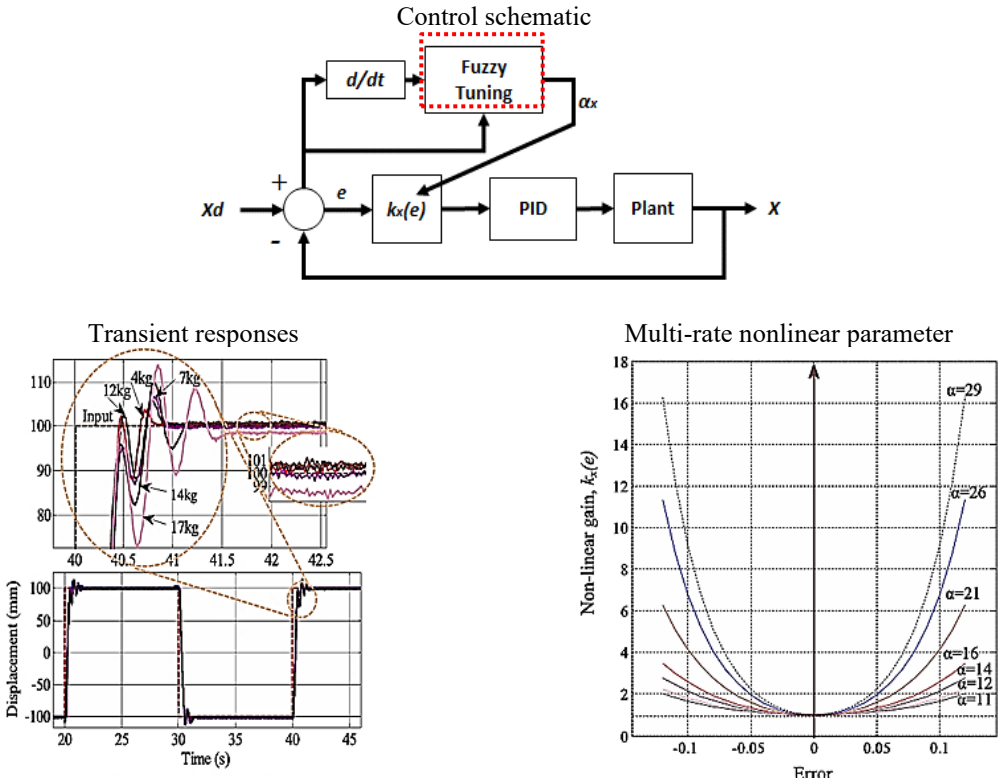

Figure 14. Robust PID-based strategy by Mostafa *et al*. [43]

The computational complexity and burden reduction have been a topic in research, and real-time industrial implementation is such an added strength. Figure 15 shows the comparison of computational load between SIFL in Figure 15(a) and FL in Figure 15(b) during the experimental validation. It clearly shows that the computational time, which is equivalent to 0.526 sec for SIFL, is faster than computational time for FL which equals 74.041 sec with the same number of programming line calls (144003 lines). The factor consolidates the lower computational load advantage. Research by Mostafa *et al*. [44] and Vieira *et al*. [45] has shown that implementing a low-cost microprocessor-based PC such as Raspberry Pi with MATLAB and Simulink onboard is highly successful. Therefore, moving forward, implementing the proposed strategy in this research is highly practical. To add with the industrial application factor, education and research alone has been bridging between lab research and low-cost industrial application [46]. As SIFL has been demonstrated to drastically lower the calculation complexity by around 35 percent (and up to around 80 to 90 percent in other research [38], [40]), integration of the structure is an absolute advantage.

Continuing on the topic of controller robustness, another PID-based research by Ning and Bone [24] also achieved robust controller performance by designing a pressure velocity acceleration (PVA) controller. The adaptivity is obtained via the acceleration feedback module, as shown in Figure 16. In addition to the benchmarked PV (without the acceleration feedback) controller, and the simple formulation of the PVA controller is shown in (20) and (21).

Path	Time Plot (Dark Band = Self Time)	Total Time (s)	Self Time (s)	Number of Calls
FLC		78.798	0.517	720006
Output Sample Points		0.000	0.000	5
Evaluate Rule Antecedents		2.947	2.947	1440013
Evaluate Rule Consequents		74.041	74.041	1440013
Defuzzify Outputs		1.292	1.292	1440013

(a)

Path	Time Plot (Dark Band = Self Time)	Total Time (s)	Self Time (s)	Number of Calls
ASSYMMETRICAL SIFLC		2.632	0.358	720006
Evaluate Rule Antecedents		1.262	1.262	1440013
Evaluate Rule Consequents		0.526	0.526	1440013
Defuzzify Outputs		0.486	0.486	1440013
Output Sample Points		0.000	0.000	5

(b)

Figure 15. MATLAB's simulink Profiler: CPUs require calculational time (a) FL and (b) SIFL

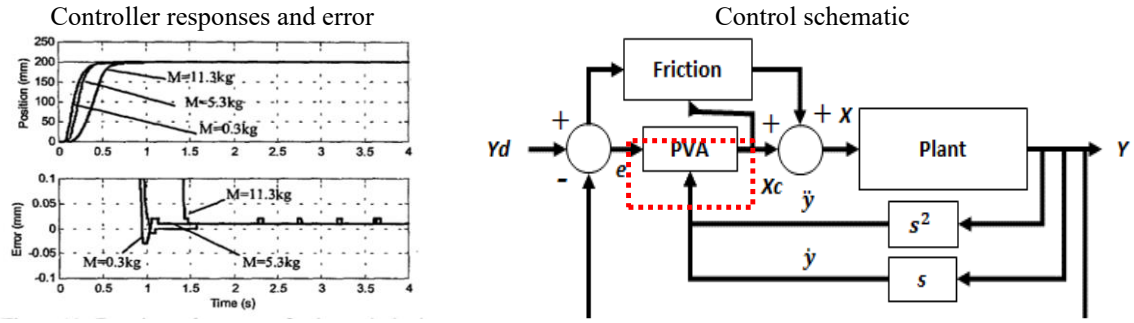

Figure 16. PVA controller; a PID-based strategy by Ning and Bone [24]

In this discussion, the control strategies achieve robust performance in both simulation and experiment when supported by a well-targeted adaptivity module (such as the SIFL). Effective adaptation must focus on the disturbance-sensitive parameters within the control algorithm to ensure meaningful compensation. The stated requirement aligns with prior findings and this research, strengthening the observations through combined mathematical robustness analysis and experimental validation. Overall, the study confirms that a properly structured adaptive component is essential for maintaining high-performance tracking under varying conditions.

$$X(s) = K_p E(s) - K_v sY(s) - K_a s^2 Y(s) \tag{20}$$

$$E(s) = Y_d(s) - Y(s) \tag{21}$$

4. CONCLUSION

The proposed T-NPID+SIFL control strategy has demonstrated strong effectiveness in achieving both precise positioning and robust performance for servo pneumatic actuator systems. The improvement gained for the T-NPID+SIFL transient rise time and a multi-step IAE index under no load disturbance, is 71.381% and 68.854%, respectively, compared to a classical SMC, in addition to comparing the strategy to a baseline nonlinear-hyperbolic PID (NH-PID), at no load disturbance the steady-state error and the overshoot also improved by 74.797% and 15.385% respectively. Beyond outperforming the classical SMC, as well as the developed NH-PID and T-NPID controllers under 1 kg, 5 kg, and 9 kg external disturbances (thereby improving the controller's practical feasibility in industrial settings). The proposed algorithm is particularly suitable for applications requiring improved critical damping response and high-precision operation. Another key contribution lies in the introduction of a variable nonlinear hyperbolic parameter structure governed by a reduced derivative action and an adaptive SIFL module. MATLAB-based simulations further reveal that the SIFL computation time is significantly lower than that of a typical dual-input fuzzy logic controller,

rendering the proposed approach computationally efficient. The improved efficiency (equivalent to that of a conventional FL controller by up to approximately 35%) makes the controller highly suitable for implementation on low-cost, dedicated microprocessors such as the Raspberry Pi, which has been successfully utilised in previous pneumatic control studies. Extending the implementation to microcontrollers (not limited to) such as Arduino may further reduce production costs for lightweight and less safety-critical applications. Moreover, higher-cost and safety-critical applications, such as underwater vehicle control, have also demonstrated successful deployment using the core SIFL structure. Additionally, the structural flexibility of the SIFL module enables various integration possibilities, which, in this work, include its utilization to modulate a nonlinear hyperbolic function, among others. Therefore, this work serves as a foundation for broader future exploration within the domain of servo pneumatic control.

Future work will focus on evaluating the robustness of the T-NPID+SIFL controller under sinusoidal and smooth curved trajectory inputs. Such trajectories reflect more realistic robotic arm motions and are essential for continuous path tracking in real-world pneumatic robotic applications. A comprehensive analysis of error convergence and stability characteristics, including the asymptotic tracking region (ATR), will further establish the stability and reliability of the proposed controller.

ACKNOWLEDGEMENTS

The authors extend their sincere gratitude to Fakulti Teknologi dan Kejuruteraan Industri dan Pembuatan (FTKIP), UTeM for supporting this research. The authors would like to acknowledge the financial support provided by the Ministry of Higher Education (MOHE) of Malaysia through the Fundamental Research Grant Scheme (FRGS), No: FRGS/1/2024/FTKIP/F00570, and Universiti Teknikal Malaysia Melaka (UTeM), with reference number FRGS/1/2024/FTKIP/F00570 and PJP/2024/FTKIP/PERINTIS/SA0022.

FUNDING INFORMATION

The authors would like to acknowledge the financial support provided by the Ministry of Higher Education (MOHE) of Malaysia through the Fundamental Research Grant Scheme (FRGS), No: FRGS/1/2024/FTKIP/F00570, and Universiti Teknikal Malaysia Melaka (UTeM), with reference number FRGS/1/2024/FTKIP/F00570 and PJP/2024/FTKIP/PERINTIS/SA0022.

AUTHOR CONTRIBUTIONS STATEMENT

This journal uses the Contributor Roles Taxonomy (CRediT) to recognize individual author contributions, reduce authorship disputes, and facilitate collaboration.

Name of Author	C	M	So	Va	Fo	I	R	D	O	E	Vi	Su	P	Fu
Khairun Najmi Kamaludin	✓	✓	✓	✓	✓	✓	✓	✓	✓	✓	✓		✓	
Lokman Abdullah	✓	✓		✓		✓		✓	✓	✓		✓	✓	✓
Syed Najib Syed Salim		✓	✓		✓		✓		✓	✓			✓	
Zamberi Jamaludin		✓		✓		✓	✓			✓	✓			
Mohd Nazmin Maslan		✓								✓				
Mohd Shahrieel Mohd Aras		✓				✓		✓		✓	✓			
Mohd Fua'ad Rahmat	✓			✓						✓	✓			
Arief Suardi Nur Chairat				✓	✓	✓		✓		✓				

C : **C**onceptualization
M : **M**ethodology
So : **So**ftware
Va : **Va**lidation
Fo : **Fo**rmal analysis
I : **I**nvestigation
R : **R**esources
D : **D**ata Curation
O : Writing - **O**riginal Draft
E : Writing - Review & **E**diting
Vi : **Vi**sualization
Su : **Su**pervision
P : **P**roject administration
Fu : **Fu**nding acquisition

CONFLICT OF INTEREST STATEMENT

The authors declare that there are no conflicts of interest, whether financial, personal, or professional, that could have influenced the research presented in this paper.

DATA AVAILABILITY

The data that support the findings of this study are available upon request to the corresponding author, Lokman Abdullah.

REFERENCES

[1] P. Beater, *Pneumatic drives*. 2007. doi: 10.1007/978-1-349-01197-1_8.
[2] P. Joji, *Pneumatic controls-(2008)*. Wiley India, 2008.
[3] S. Dudić, V. Reljić, D. Šešlija, N. Dakić, and V. Blagojević, "Improving energy efficiency of flexible pneumatic systems," *Energies (Basel).*, vol. 14, no. 7, Apr. 2021, doi: 10.3390/en14071819.
[4] S. N. S. Salim, "Modeling and control design of an industrial pneumatic actuator system." 2014.
[5] C. Canudas de Wit, H. Olsson, K. J. Astrom, and P. Lischinsky, "A new model for control of systems with friction," *IEEE Transactions on Automatic Control*, vol. 40, no. 3, pp. 419–425, Mar. 1995, doi: 10.1109/9.376053.
[6] T. Raparelli, A. Manuello Bertetto, and L. Mazza, "Experimental and numerical study of friction in an elastomeric seal for pneumatic cylinders," *Tribology International*, vol. 30, no. 7, pp. 547–552, Jul. 1997, doi: 10.1016/S0301-679X(97)00015-7.
[7] F. Soleymani, S. M. Rezaei, S. Sharifi, and M. Zareinejad, "Position control of a servo-pneumatic actuator using generalized Maxwell-Slip friction model," in *2016 4th International Conference on Robotics and Mechatronics (ICROM)*, Oct. 2016, pp. 246–251. doi: 10.1109/ICRoM.2016.7886854.
[8] D. Saravanakumar, B. Mohan, and T. Muthuramalingam, "A review on recent research trends in servo pneumatic positioning systems," *Precision Engineering*, Jul. 2017, doi: 10.1016/j.precisioneng.2017.01.014.
[9] R. Richardson, A. R. Plummer, and M. D. Brown, "Self-tuning control of a low-friction pneumatic actuator under the influence of gravity," *IEEE Transactions on Control Systems Technology*, vol. 9, no. 2, pp. 330–334, Mar. 2001, doi: 10.1109/87.911384.
[10] P. Qian, L. Liu, C. Pu, D. Meng, and L. M. R. Páez, "Methods to improve motion servo control accuracy of pneumatic cylinders - review and prospect," *International Journal of Hydromechatronics*, vol. 6, no. 3, pp. 274–310, 2023, doi: 10.1504/IJHM.2023.132301.
[11] X. Gao and Z.-J. Feng, "Design study of an adaptive Fuzzy-PD controller for pneumatic servo system," *Control Engineering Practice*, vol. 13, no. 1, pp. 55–65, Jan. 2005, doi: 10.1016/j.conengprac.2004.01.001.
[12] M. Farag and N. Z. Azlan, "Adaptive backstepping position control of pneumatic anthropomorphic robotic hand," *Procedia Computer Science*, vol. 76, no. Iris, pp. 161–167, 2015, doi: 10.1016/j.procs.2015.12.334.
[13] B. Yao and M. Tomizuka, "Adaptive robust control of SISO nonlinear systems in a semi-strict feedback form," *Automatica*, vol. 33, no. 5. pp. 893–900, 1997. doi: 10.1016/S0005-1098(96)00222-1.
[14] Bin Yao, "High performance adaptive robust control of nonlinear systems: a general framework and new schemes," *Proceedings of the 36th IEEE Conference on Decision and Control*, vol. 3, pp. 2489–2494, 1997, doi: 10.1109/CDC.1997.657530.
[15] D. Meng, G. Tao, and X. Zhu, "Integrated direct/indirect adaptive robust motion trajectory tracking control of pneumatic cylinders," *International Journal of Control*, vol. 86, no. 9, pp. 1620–1633, Sep. 2013, doi: 10.1080/00207179.2013.792002.
[16] D. Meng, G. Tao, and X. Zhu, "Adaptive robust motion trajectory tracking control of pneumatic cylinders," *Journal of Central South University*, vol. 20, no. 12, pp. 3445–3460, Dec. 2013, doi: 10.1007/s11771-013-1869-0.
[17] D. Meng, G. Tao, H. Liu, and X. Zhu, "Adaptive robust motion trajectory tracking control of pneumatic cylinders with lugre model-based friction compensation," *Chinese Journal of Mechanical Engineering (English Edition)*, vol. 27, no. 4, pp. 802–815, 2014, doi: 10.3901/CJME.2014.0430.085.
[18] A. Ayadi, S. Hajji, M. Smaoui, and A. Chaari, "Chattering-free adaptive sliding mode control for pneumatic system position tracking," in *2015 16th International Conference on Sciences and Techniques of Automatic Control and Computer Engineering (STA)*, Dec. 2015, pp. 752–757. doi: 10.1109/STA.2015.7505126.
[19] H.-P. Ren, X. Wang, J.-T. Fan, and O. Kaynak, "Fractional order sliding mode control of a pneumatic position servo system," *Journal of the Franklin Institute*, vol. 356, no. 12, pp. 6160–6174, Aug. 2019, doi: 10.1016/j.jfranklin.2019.05.024.
[20] M. C. Hidalgo and C. Garcia, "Friction compensation in control valves: Nonlinear control and usual approaches," *Control Engineering Practice*, vol. 58, pp. 42–53, Jan. 2017, doi: 10.1016/j.conengprac.2016.09.011.
[21] R. P. Borase, D. K. Maghade, S. Y. Sondkar, and S. N. Pawar, "A review of PID control, tuning methods and applications," *International Journal of Dynamics and Control*, vol. 9, no. 2, pp. 818–827, Jun. 2021, doi: 10.1007/s40435-020-00665-4.
[22] S. Bennett, *A history of control engineering 1930-1955*. 1993. doi: 10.1049/pbce047e.
[23] S. Jamian, S. N. S. Salim, S. C. K. Junoh, M. N. Kamarudin, and L. Abdullah, "Nonlinear proportional integral (NPI) double hyperbolic controller for pneumatic actuator system," 2020, pp. 221–229. doi: 10.1007/978-981-15-1289-6_21.
[24] S. Ning and G. M. Bone, "High steady-state accuracy pneumatic servo positioning system with PVA/PV control and friction compensation," in *Proceedings-IEEE International Conference on Robotics and Automation*, 2002, vol. 3, no. May, pp. 2824–2829. doi: 10.1109/ROBOT.2002.1013660.
[25] Z. Situm, D. Pavkovic, and B. Novakovic, "Servo pneumatic position control using fuzzy PID gain scheduling," *Journal of Dynamic Systems, Measurement and Control, Transactions of the ASME*, vol. 126, no. 2, pp. 376–387, Jun. 2004, doi: 10.1115/1.1767857.
[26] K. N. Kamaludin *et al.*, "Triple nonlinear hyperbolic PID with static friction compensation for precise positioning of a servo pneumatic actuator," *IIUM Engineering Journal*, vol. 24, no. 2, pp. 315–336, Jul. 2023, doi: 10.31436/iiumej.v24i2.2766.
[27] G. Filo, "A review of fuzzy logic method development in hydraulic and pneumatic systems," *Multidisciplinary Digital Publishing Institute (MDPI)*, Nov. 2023, doi: 10.3390/en16227584.
[28] M. I. P. Azahar, A. Irawan, and R. M. T. R. Ismail, "Self-tuning hybrid fuzzy sliding surface control for pneumatic servo system positioning," *Control Engineering Practice*, vol. 113, p. 104838, 2021, doi: 10.1016/j.conengprac.2021.104838.
[29] B.-J. Choi, S.-W. Kwak, and B. K. Kim, "Design of a single-input fuzzy logic controller and its properties," *Fuzzy Sets and Systems*, vol. 106, no. 3, pp. 299–308, Sep. 1999, doi: 10.1016/S0165-0114(97)00283-2.
[30] L. Ljung, "Technical report from automatic control at Linköpings universitet perspectives on system identification perspectives on system identification," 2008.
[31] H. Seraji, "A new class of nonlinear PID controllers with robotic applications," *Journal of Robotic Systems*, vol. 15, no. 3, pp. 161–181, Mar. 1998, doi: 10.1002/(SICI)1097-4563(199803)15:3<161::AID-ROB4>3.0.CO;2-O.
[32] T. H. Chiew, Z. Jamaludin, A. Y. B. Hashim, N. A. Rafan, and L. Abdullah, "Identification of friction models for precise positioning system in machine tools," in *Procedia Engineering*, 2013, vol. 53, pp. 569–578. doi: 10.1016/j.proeng.2013.02.073.
[33] K. N. Kamaludin and Others, "Performance evaluation of an adaptive sigmoid friction compensation for pneumatic trajectory," in

Institute of Electrical and Electronics Engineers (IEEE), Jun. 2023, pp. 165–171. doi: 10.1109/iccre57112.2023.10155570.
[34] Z. Jamaludin, "Disturbance compensation for machine tools with linear motor drives (storingsonderdrukking voor werktuigmachines met lineaire motoren)," 2008.
[35] M.-C. Shih and K.-R. Pai, "Design and nanometer positioning of a low friction pneumatic cylinder embedded with aerostatic bearings," in *Proceedings of the JFPS International Symposium on Fluid Power*, 2008, vol. 2008, no. 7–1, pp. 231–236. doi: 10.5739/isfp.2008.231.
[36] K. N. Kamaludin and Others, "Accurate and robust adaptive hyperbolic-PID control strategy for a servo pneumatic system," *Journal of Advanced Manufacturing Technology*, 2025.
[37] S. N. S. Salim, S. C. K. Junoh, L. Abdullah, and Z. Retas, "Nonlinear proportional integral (NPI) double hyperbolic controller for pneumatic actuator system," *Journal Of Advance Manufacturing Technology*, 2020.
[38] F. Taeed, Z. Salam, and S. Ayob, "FPGA implementation of a single-input fuzzy logic controller for boost converter with the absence of an external analog-to-digital converter," *IEEE Transactions on Industrial Electronics*, vol. 59, no. 2, pp. 1208–1217, Feb. 2012, doi: 10.1109/TIE.2011.2161250.
[39] T. J. Ross, *Fuzzy logic with engineering applications, third edition*, 3rd ed. Wiley, 1995.
[40] Z. Salam, F. Taeed, and S. M. Ayob, "Design and implementation of a single input fuzzy logic controller for boost converters," *Journal of Power Electronics*, vol. 11, no. 4, 2011, doi: 10.6113/JPE.2011.11.4.542.
[41] L. Abdullah, Z. Jamaludin, T. H. Chiew, N. A. Rafan, and M. Y. Yuhazri, "Extensive tracking performance analysis of classical feedback control for XY stage ballscrew drive system," *Applied Mechanics and Materials*, vol. 229--231, pp. 750–755, 2012, doi: 10.4028/www.scientific.net/AMM.229-231.750.
[42] S. N. Syed Salim, M. F. Rahmat, A. 'Athif Mohd Faudzi, Z. H. Ismail, and N. Sunar, "Position control of pneumatic actuator using self-regulation nonlinear PID," *Mathematical Problems in Engineering*, vol. 2014, no. 1, Jan. 2014, doi: 10.1155/2014/957041.
[43] S. N. S. Salim, M. F. ad Rahmat, A. A. M. Faudzi, Z. H. Ismail, N. H. Sunar, and S. A. Samsudin, "Robust control strategy for pneumatic drive system via enhanced nonlinear PID controller," *International Journal of Electrical and Computer Engineering*, vol. 4, no. 5, pp. 658–667, 2014, doi: 10.11591/ijece.v4i5.6853.
[44] S. Mostafa, A. Zekry, A. Youssef, and W. R. Anis, "Raspberry Pi design and hardware implementation of fuzzy-PI controller for three-phase grid-connected inverter," *Energies (Basel).*, vol. 15, no. 3, Feb. 2022, doi: 10.3390/en15030843.
[45] G. Vieira, J. Barbosa, P. Leitao, and L. Sakurada, "Low-cost industrial controller based on the Raspberry Pi platform," in *2020 IEEE International Conference on Industrial Technology (ICIT)*, Feb. 2020, pp. 292–297. doi: 10.1109/ICIT45562.2020.9067148.
[46] J. Sobota, R. P\visl, P. Balda, and M. Schlegel, "Raspberry pi and Arduino boards in control education," in *IFAC Proceedings Volumes (IFAC-PapersOnline)*, 2013, pp. 7–12. doi: 10.3182/20130828-3-UK-2039.00024.

BIOGRAPHIES OF AUTHORS

Khairun Najmi Kamaludin received his degree in electrical engineering in mechatronics from Universiti Teknologi Malaysia (UTM) in 2006. Upon completing the degree, he worked at a few multinational manufacturing companies specializing in manufacturing equipment, equipment automation, and tooling engineering for 10 years. In 2019, he completed his master's in manufacturing system engineering with Universiti Teknikal Malaysia Melaka (UTeM). He is currently completing his thesis in servo pneumatic control system under the Advance Mechatronics Laboratory, Fakulti Teknologi dan Kejuruteraan Industri dan Pembuatan (FTKIP), UTeM. He can be reached via email at p052010004@student.utem.edu.my.

Lokman Abdullah received the B.Eng. degree in manufacturing engineering from International Islamic University of Malaysia (IIUM) in 2005, the M.Sc. degree in Manufacturing Systems Engineering from Coventry University, UK, in 2008, and the Ph.D. degree in Engineering from Universiti Teknikal Malaysia Melaka (UTeM), Malaysia, in 2014. He is currently an Associate Professor with the Department of Robotics and Automation, Faculty of Industrial and Manufacturing Technology and Engineering, Universiti Teknikal Malaysia Melaka, Malaysia. His fields of interest are control systems, motion control, mechatronics, and industrial automation. He can be reached via email at lokman@utem.edu.my.

Syed Najib Syed Salim received his M.Eng. in electrical engineering from Universiti Teknologi Malaysia in 2003 and later earned his Ph.D. in Electrical Engineering, specializing in Control System Engineering, from the same institution in 2015. He is currently a Senior Lecturer at the Faculty of Electrical Technology and Engineering at Universiti Teknikal Malaysia Melaka, specializing in control systems design, mechatronics, instrumentation, and industrial automation. His research interests include nonlinear PID controllers, intelligent control systems, and industrial automation techniques. Syed Najib has published several papers in international journals and conferences, contributing significantly to the fields of control systems and industrial automation. He can be reached via email at syednajib@utem.edu.my.

Zamberi Jamaludin received his bachelor's degree in chemical engineering from Lakehead University, Canada, in 1997, before completing his Master of Engineering (Manufacturing System) from National University of Malaysia in 2001. In 2008, he completed his Ph.D. study in the field of Control Engineering from Katholieke Universiteit Leuven, Belgium. He is currently a Professor at the Faculty of Industrial and Manufacturing Technology and Engineering, Universiti Teknikal Malaysia Melaka (UTeM), Malaysia, since 2002. His areas of specialization are control systems, robotics, automation, and machining. He can be contacted at zamberi@utem.edu.my.

Mohd Nazmin Maslan received the B.Eng. from Universiti Teknologi PETRONAS (UTP), Malaysia, in 2009, the M.Eng. degree from Universiti Teknologi Malaysia (UTM), Malaysia, in 2012, and the Dr. Eng. degree from Tokyo Institute of Technology (Tokyo Tech), Japan, in 2018. In 2010, he was a Research Assistant at the Faculty of Health Science and Biomedical Engineering, UTM. He is currently a Senior Lecturer at the Faculty of Industrial and Manufacturing Technology and Engineering, Universiti Teknikal Malaysia Melaka (UTeM), and more recently a Coordinator under Unit STEM in Pusat Pengurusan Kolaborasi RICE UTeM, Melaka. His current research interests are in precision mechatronics and precision motion control. He can be contacted at nazmin@utem.edu.my.

Mohd Shahrieel Mohd Aras received his M.Eng. in electrical engineering from Universiti Teknologi Malaysia in 2006 and later earned his Ph.D. in Electrical Engineering, specializing in Control System Engineering, from the same institution in 2015. Mohd Shahrieel Mohd Aras is an Associate Professor in the Department of Mechatronic Engineering at the Technical University of Malaysia Malacca (UTeM). He specializes in robotics, with a particular focus on underwater robotics, fuzzy logic systems, and control systems. He is a highly prolific researcher and mentor, contributing significantly to the academic literature. He has co-authored over 150 academic publications, including numerous papers in international journals and conference proceedings. He can be contacted at shahrieel@utem.edu.my.

Mohd Fua'ad Rahmat received his degree in electrical engineering at Universiti Teknologi Malaysia in 1989. He started his master's degree by taught course specialized in Control System Engineering and graduated in 1993 at The University of Sheffield, UK. Subsequently, he pursued his Ph.D. degree in Electronic Instrumentation Engineering at the School of Engineering, Sheffield Hallam University, UK, and graduated in 1996. Currently, he is a Professor in the Department of Control and Mechatronics Engineering, Faculty of Electrical Engineering, Universiti Teknologi Malaysia Skudai, Johor. His fields of specialization include system identification and estimation, signal processing, process tomography for industrial process, process control instrumentation, sensors and actuators, and hydraulic and pneumatic systems. He can be reached via email at fuaad@utm.my or fuaad@utm.edu.my.

Arief Suardi Nur Chairat received his bachelor's degree in industrial engineering and his master's degree in industrial engineering and management from the Institut Teknologi Bandung (ITB), Indonesia. He is currently a Lecturer at the Institut Teknologi PLN (ITPLN), Jakarta, under the Faculty of Technology and Energy Business. He has served in several academic leadership roles within the faculty. He is presently pursuing his Doctoral degree at Universiti Teknikal Malaysia Melaka (UTeM), focusing on research in energy systems optimization, renewable energy integration, marginal abatement cost modelling, and sustainable industrial systems. He can be reached via email at arief.suardi@itpln.ac.id.